Journal of Alloys and Compounds 509 (2011) 141–146

Contents lists available at ScienceDirect

Journal of Alloys and Compounds

journal homepage: www.elsevier.com/locate/jallcom

# Dependence of magnetic properties on the film thickness and Pt atomic fraction of post-annealed $Fe_{1-x}Pt_x$-C granular films on MgO(1 0 0) and $SiO_2$/Si(1 0 0) substrates

W.B. Mi*, J. Jin, H.L. Bai

*Tianjin Key Laboratory of Low Dimensional Materials Physics and Preparing Technology, Institute of Advanced Materials Physics, Faculty of Science, Tianjin University, Tianjin 300072, China*

ARTICLE INFO

*Article history:*
Received 8 July 2010
Received in revised form 30 August 2010
Accepted 1 September 2010
Available online 16 September 2010

*PACS:*
75.75.−c
75.70.−i
75.70.Ak
75.50.−y

*Keywords:*
Granular films
FePt
Magnetocrystalline anisotropy
Magnetic properties

ABSTRACT

The $Fe_{1-x}Pt_x$-C granular films with different Pt atomic fractions ($0.09 \le x \le 0.52$) and film thicknesses ($5\,nm \le t \le 100\,nm$) were deposited on MgO(1 0 0) and $SiO_2$/Si(1 0 0) substrates by facing-target sputtering and post-annealing. With the increasing $x$, the ordered $L1_0$ FePt grains form. All of the films are ferromagnetic, and the easy axis is in the film plane. With the decrease of $t$, the films turn from hard ferromagnetic to soft ferromagnetic. The maximum coercivity of the 100-nm thick $Fe_{1-x}Pt_x$-C granular films measured at a 10-kOe field is 3.7 kOe at $x = 0.48$. The coercivity of the $Fe_{0.56}Pt_{0.44}$-C granular films increases, and the magnetization measured at a 10-kOe field decreases with the increasing $t$. The reversal mechanism of the 100-nm thick $Fe_{1-x}Pt_x$-C granular films turns from the domain wall motion to the Stoner–Wohlfarth rotation mode as $x$ increases. However, the reversal mechanism of the $Fe_{56}Pt_{44}$-C granular films with different $t$ approaches the Stoner–Wohlfarth rotation mode, and is film-thickness independent.



## 1. Introduction

The size of the recorded units should decrease due to the increasing recording density and the number of the grains packed in a bit cell should increase to maintain the signal-to-noise ratio. For obtaining high area densities of 1 Tbit/in$^2$, the CoCrPt based perpendicular magnetic recording media are unable to be the medium because the magnetocrystalline anisotropy of the CoCrPt alloy is not large enough. The face-centered tetragonal (fct) FePt alloy with a short $c$ axis has a large saturation magnetization of 1100 emu/cm$^3$ and a high magnetocrystalline anisotropy of $7.0 \times 10^7$ erg/cm$^3$ due to the atomic arrangement with alternating Fe and Pt layers along the $c$ axis [1–7]. Therefore, the fct FePt alloy becomes the potential candidate of the high density perpendicular magnetic recording media. Generally, the FePt films fabricated by sputtering at the low substrate temperatures have a disordered face-centered-cubic (fcc) structure. Annealing at high temperatures above 500 °C is necessary for the FePt grains to transform from the disordered phase to the ordered fct structure [8–11]. Recently, the nonmagnetic matrixes including C, $SiO_2$, $TiO_2$, $Ta_2O_5$ and $SiN_x$ have been used to isolate the FePt grains for decreasing the signal-to-noise ratio [12–16]. The metal elements such as Cr, Cu, Ru and Ag were added in the FePt alloy to improve the phase transition and the ordering of the fct phase [17–20]. Meanwhile, multiple laser pulsing and ultrafast heating were used to make the phase transition into the ordered fct FePt phase [21,22]. Furthermore, the lattice of the substrates and underlayers can also affect the ordering and the phase transition of the FePt films [23,24]. As a candidate that could serve as the matrix to separate the ferromagnetic nanoparticles, C is particularly attractive because it can prevent surface oxidation of the particles and provide magnetic isolation among the neighboring particles, which can reduce interparticle exchange coupling and hence reduce the recording noise [25,26]. Therefore, the magnetic properties of the FePt based granular films with large coercivity and well phase segregation should be interesting for the practical application in the field of the high density magnetic recording media. In this paper, $Fe_{1-x}Pt_x$-C granular films with different Pt atomic fractions and film thicknesses were fabricated by sputtering and post-annealing. The structure and magnetic properties of the films were investigated systematically.

* Corresponding author.
*E-mail address:* miwenbo@tju.edu.cn (W.B. Mi).

0925-8388/$ – see front matter © 2010 Elsevier B.V. All rights reserved.
doi:10.1016/j.jallcom.2010.09.009

## 2. Experimental details

$Fe_{1-x}Pt_x$-C granular films with different Pt atomic fractions ($0.09 \le x \le 0.52$) and film thicknesses ($5\,nm \le t \le 100\,nm$) were fabricated on MgO(1 0 0) and $SiO_2$/Si(1 0 0) wafers using a DC facing-target sputtering system without substrate heating. The film thickness of the films with different $x$ is 100 nm, and the Pt atomic fraction $x$ of the films with different $t$ is 0.48. When the base pressure of the chamber reaches $6.0 \times 10^{-4}$ Pa or better, Ar (99.999%) gas was introduced into the chamber till 1.0 Pa. One of the facing targets was graphite (99.99%) and the other was pure Fe (99.999%) target on which pure Pt (99.99%) pieces were placed. The film thickness was determined using a Dektak 6M surface profiler. The as-deposited $Fe_{1-x}Pt_x$-C granular films were subsequently annealed at 550 °C for 2 h in the chamber with $10^{-6}$ Pa. The atomic fraction of Fe, Pt and C elements was measured using an energy dispersive X-ray spectrometer (EDX), and the C atomic fraction in the films was about 61% with an error of 3%. The surface morphology and microstructure of the films were characterized using a scanning electron microscope (SEM, Hitachi S-4800) working at 20 kV, an X-ray diffractometer (XRD, D/max-2500×, Cu Kα, wavelength 0.1504 nm), The magnetic properties of the films were measured using a vibrating sample magnetometer (VSM, LDJ9600–1) under a 10-kOe field at room temperature.

## 3. Results and discussion

All of the as-deposited films are amorphous because the substrate temperature is too low for Fe, Pt and C atoms to crystallize during the film deposition. In order to make the films crystallize, the as-deposited films were annealed at 550 °C for 2 h in the chamber with $10^{-6}$ Pa. Fig. 1 shows the XRD patterns of the 100-nm

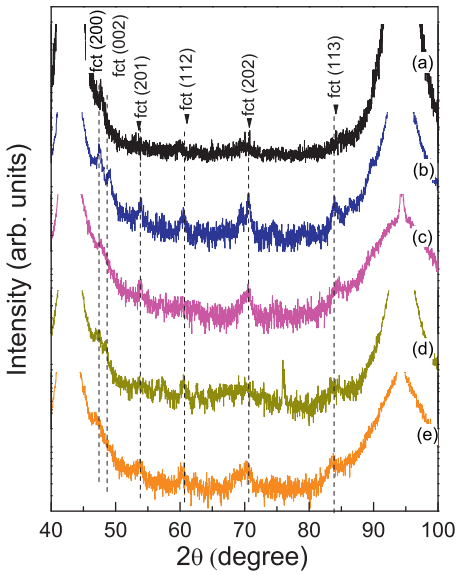


**Fig. 1.** XRD patterns of the 100-nm thick $Fe_{1-x}Pt_x$-C granular films on MgO(1 0 0) substrates annealed at 550 °C, (a) $x = 0.18$, (b) $x = 0.27$, (c) $x = 0.44$, (d) $x = 0.48$, and (e) $x = 0.52$.

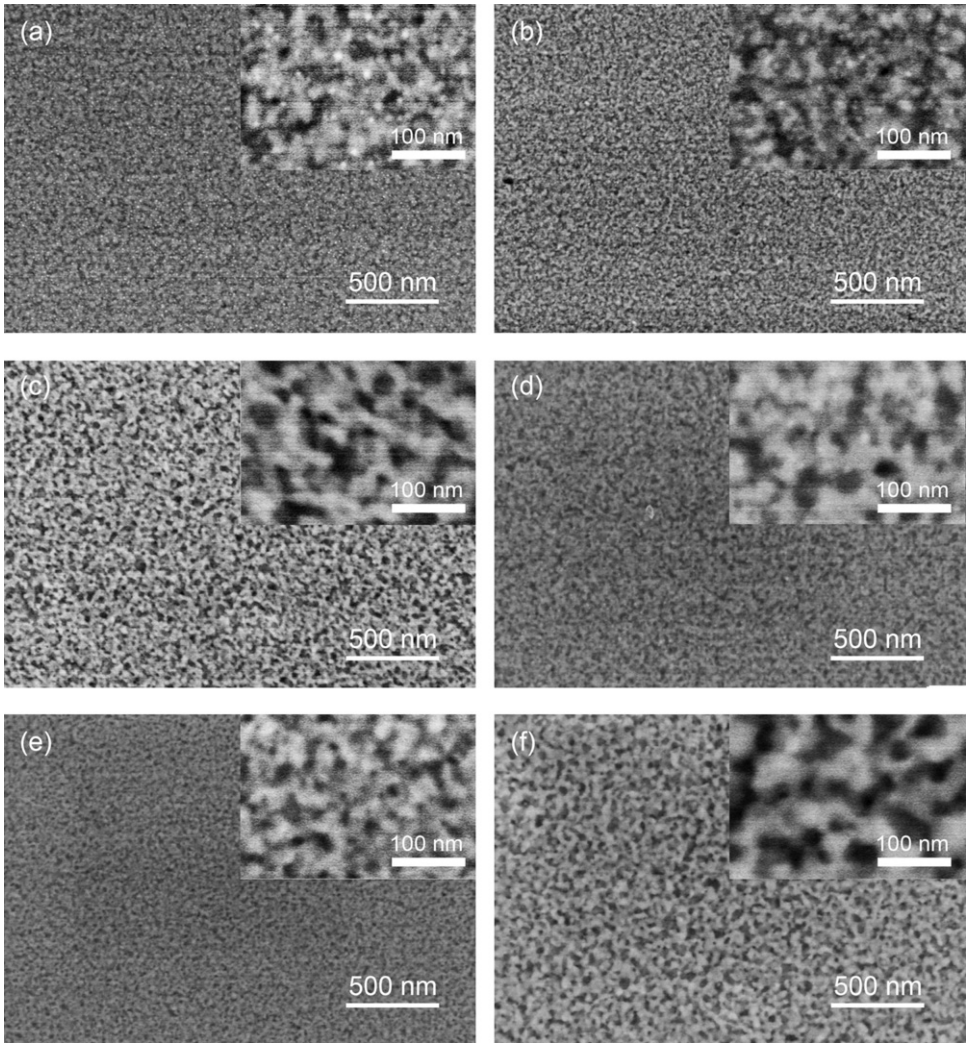


**Fig. 2.** SEM images of the 100-nm thick $Fe_{1-x}Pt_x$-C granular films on $SiO_2$/Si(1 0 0) substrates annealed at 550 °C, (a) $x = 0.09$, (b) $x = 0.18$, (c) $x = 0.27$, (d) $x = 0.44$, (e) $x = 0.48$, and (f) $x = 0.52$.

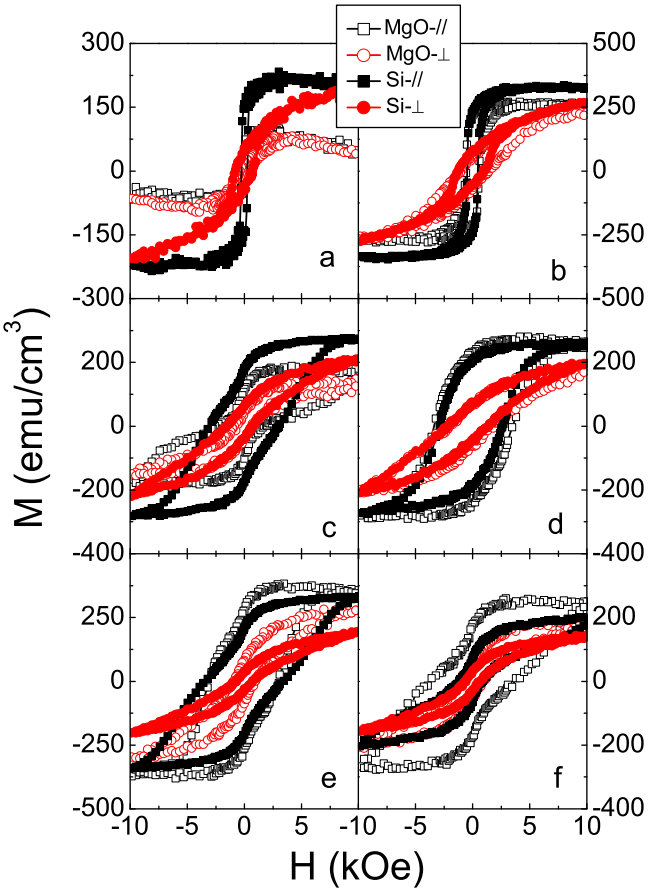


**Fig. 3.** *M–H* curves of the 100-nm thick $Fe_{1-x}Pt_x$-C granular films annealed at 550 °C, (a) $x = 0.09$, (b) $x = 0.18$, (c) $x = 0.27$, (d) $x = 0.44$, (e) $x = 0.48$, and (f) $x = 0.52$.

thick $Fe_{1-x}Pt_x$-C granular films on MgO(1 0 0) substrates annealed at 550 °C. In Fig. 1, the intensity of the diffraction peaks is weak because the films are composite ones but not continuous ones. Meanwhile, all of the films are polycrystalline. From Fig. 1(a), it is clear that the position of the diffraction peaks is lower than that of the standard fct FePt lattice due to the low Fe atomic fractions, suggesting that the lattice constant *c* does not become less than *a* and *b*. In Fig. 1(b), the diffraction peaks at the positions lower than that of the standard fct FePt lattice can be observed except for the diffraction peaks from the ordered fct FePt grains, revealing that there are two phases with different lattice constants in the films. In Fig. 1(c)–(e), the diffraction peaks are from the ordered fct FePt grains due to the formation of the ordered fct FePt grains. Therefore, the above XRD results show that the ordered fct FePt grains form in the films with $x \geq 0.44$ after being annealed at 550 °C. In Fig. 1, some diffraction peaks are not from the fct phase, which should be from the substrates because sometimes these peaks can be observed when we measured the XRD spectra of the substrates without the films.

Fig. 2 gives the SEM images of the 100-nm thick $Fe_{1-x}Pt_x$-C granular films on $SiO_2$/Si(1 0 0) substrates annealed at 550 °C. From Fig. 2, it is clear that all the films are composed of white and dark regions even though the size of these regions is dependent on *x*. In Fig. 2(a) and (b), the size of the dark regions is about 20 nm, and the contract between white and dark regions is not good enough. In Fig. 2(c), the size of the dark regions is about 30 nm, and these regions are separated completely by the white regions. In Fig. 2(d), the dark regions are about 40 nm, but are not separated by the white layers. Then the size of the dark regions becomes smaller again, as shown in Fig. 2(e). However, in Fig. 2(f), as *x* increases to 0.52, the size of the dark regions increases to about 60 nm and these dark regions connect with each other.

Fig. 3 displays the *M–H* curves of the 100-nm thick $Fe_{1-x}Pt_x$-C granular films on MgO(1 0 0) and $SiO_2$/Si(1 0 0) substrates annealed at 550 °C. From Fig. 3, all of the films are ferromagnetic, and the easy axis of all the films lies in the film plane because the in-plane moments are easier to be aligned than the out-of-plane ones. In Fig. 3(a) and (b), the coercivity of the films is less than 1.0 kOe, which can be explained by the facts that there are no ordered fct FePt grains in the films with a small *x*. In Fig. 3(c), the *M–H* curves of the films with $x = 0.27$ exhibit a two-step saturation behavior. The rapidly saturated part is from the soft ferromagnetic phase, and the slowly saturated part from the hard ferromagnetic ordered fct phase. At $x = 0.44$ and 0.48, the in-plane coercivity of the films reaches about 3.5 kOe at room temperature when a 10-kOe field was applied, and no two-step saturation behavior can be observed because only the ordered fct FePt grains exist in the films, as shown in Fig. 3(d) and (e). All of the films are composed of the FePt grains embedded in C matrix, and the space distribution of the FePt grains in the matrix is random. Meanwhile, the size distribution of the FePt grains is also random. It is well known that the lattice of the ordered fct FePt has a mismatch degree of 9.7% with the lattice of the MgO(0 0 1) wafer. Therefore, when the FePt grains contact with the MgO(1 0 0) wafers, the substrate can provide the stress that can improve the ordering of the fct phase during the post-annealing. At $x = 0.52$, the in-plane coercivity of the films on the MgO(1 0 0) substrates is about 3.7 kOe, much larger than that on the $SiO_2$/Si(1 0 0) substrates. The difference can be explained by the facts that more FePt grains contact with the lattice of the MgO(1 0 0) wafer, so that the stress between the two-mismatched lattices can improve the ordering of the FePt grains. For the films with other *x*, few FePt grains contact with the MgO(1 0 0) substrates so no difference can be observed between the films on the MgO(1 0 0) and $SiO_2$/Si(1 0 0) substrates. At $x = 0.27$, the in-plane coercivity of the films on the MgO(1 0 0) substrates is much smaller than that on the $SiO_2$/Si(1 0 0) substrates, which may be ascribed to the facts that

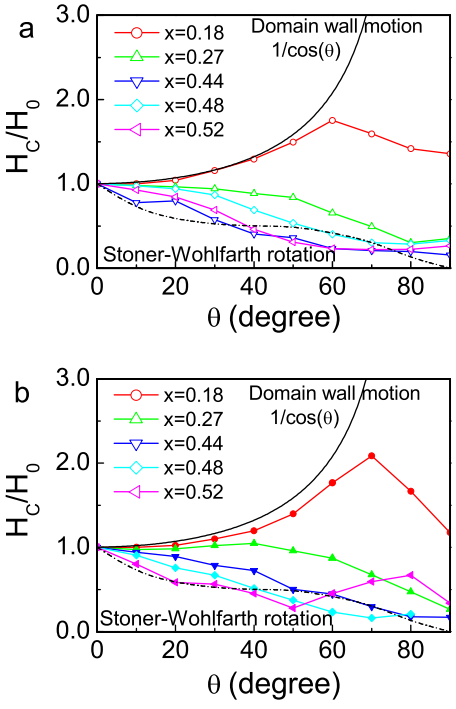


**Fig. 4.** Angular dependence of the coercivity of the 100-nm thick $Fe_{1-x}Pt_x$-C granular films annealed at 550 °C on (a) MgO(1 0 0) and (b) $SiO_2$/Si(1 0 0) substrates.

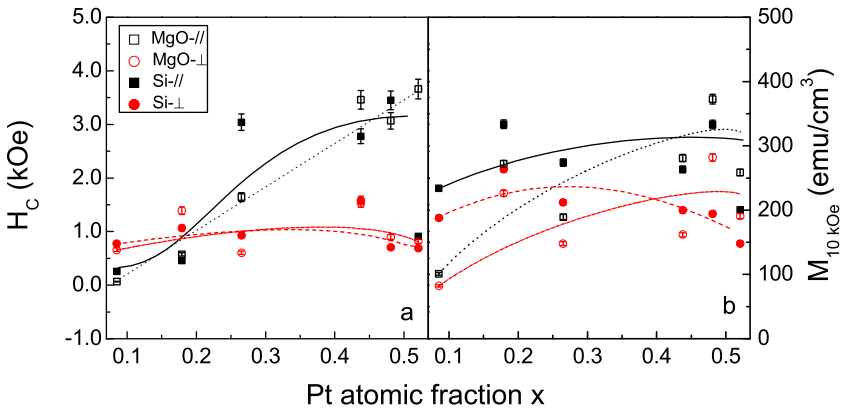


**Fig. 5.** $x$ dependence of the (a) magnetization and (b) coercivity of the 100-nm thick $Fe_{1-x}Pt_x$-C granular films annealed at 550 °C measured at a 10-kOe field. The lines are the guides to the eyes.

there are more smaller FePt grains on the MgO(1 0 0) substrates than that on the $SiO_2$/Si(1 0 0) substrates at this composition.

Fig. 4 shows the angular dependence of the coercivity of the 100-nm thick $Fe_{1-x}Pt_x$-C granular films on MgO(1 0 0) and $SiO_2$/Si(1 0 0) substrates annealed at 550 °C. It is worthy to note that the reversal mechanism of the films on the MgO(1 0 0) and $SiO_2$/Si(1 0 0) substrates changes with $x$. Ideal domain wall motion follows the $1/\cos\theta$ curve [27], where $\theta$ is the angle between the applied field and easy axis of the films (in the film plane). The reversal mechanism deviates from the domain wall motion mode and approaches Stoner–Wohlfarth (S–W) rotation mode [28] with the increasing $x$. However, the out-of-plane coercivity of all the annealed films is not zero, which does not critically follow the S–W rotation mode with zero out-of-plane coercivity. This discrepancy may be ascribed to the magnetostatic interaction between the magnetic particles that prevents the particles rotation at high angles [29].

Fig. 5 gives the $x$ dependence of the saturation magnetization and coercivity of the 550 °C annealed 100-nm thick $Fe_{1-x}Pt_x$-C granular films. From Fig. 5(a), the in-plane coercivity of the films on MgO(1 0 0) substrates increases with the increase of $x$. For the films on the $SiO_2$/Si(1 0 0) substrates, the maximum in-plane coercivity reaches about 3.5 kOe at $x = 0.48$. The out-of-plane coercivity of all the films is almost 1.0 kOe. In Fig. 5(b), the magnetization at a 10-kOe field does not satisfy a simple relation with $x$ because the magnetization of the films can be affected by the formation of different phases and the phase segregation between the magnetic particles and matrix.

For investigating the effect of the film thickness on the magnetic properties of the films, the $Fe_{56}Pt_{44}$-C granular films with different film thicknesses were fabricated and their magnetic properties were analyzed in details. Fig. 6 displays the $M$–$H$ curves of the $Fe_{56}Pt_{44}$-C granular films with different film thicknesses annealed at 550 °C. From Fig. 6, it is clear that all of the films are ferromagnetic, and the films turn from hard ferromagnetic to soft ferromagnetic with the decrease of $t$. This transition can be explained by the facts that the size of the ordered fct FePt grains decreases with the decreasing t and the magnetocrystalline anisotropy energy ($KV$) decreases so that the coercivity of the films becomes smaller, where $K$ and $V$ are the magnetocrystalline anisotropy and the volume of the ordered FePt grains, respectively. Meanwhile, the easy axis of the films with different $t$ is in the film plane. The $t$ dependence of the coercivity and magnetization at a 10-kOe field of the $Fe_{56}Pt_{44}$-C granular films annealed at 550 °C is given in Fig. 7. From Fig. 7(a), one can see that the coercivity of the films increases with the increasing $t$ below 50 nm, and saturates with further increasing $t$ above 50 nm. However, the magnetization at a 10-kOe field decreases with the increasing $t$, as shown in Fig. 7(b).

According to Arcas et al., the coercivity of any ferromagnetic sample is related to the effective magnetocrystalline anisotropy constant $K$ and the spontaneous magnetization $M_S$ by the relation of $H_c = pK/M_S$, where $p$ is a dimensionless factor depending on the particular type of magnetizing process [30,31]. For example, the S–W model gives $p = 2$ for the ideal non-interacting single domain magnetic particles with the uniaxial magnetic anisotropy [31]. Therefore, when the magnetization of the films decreases,

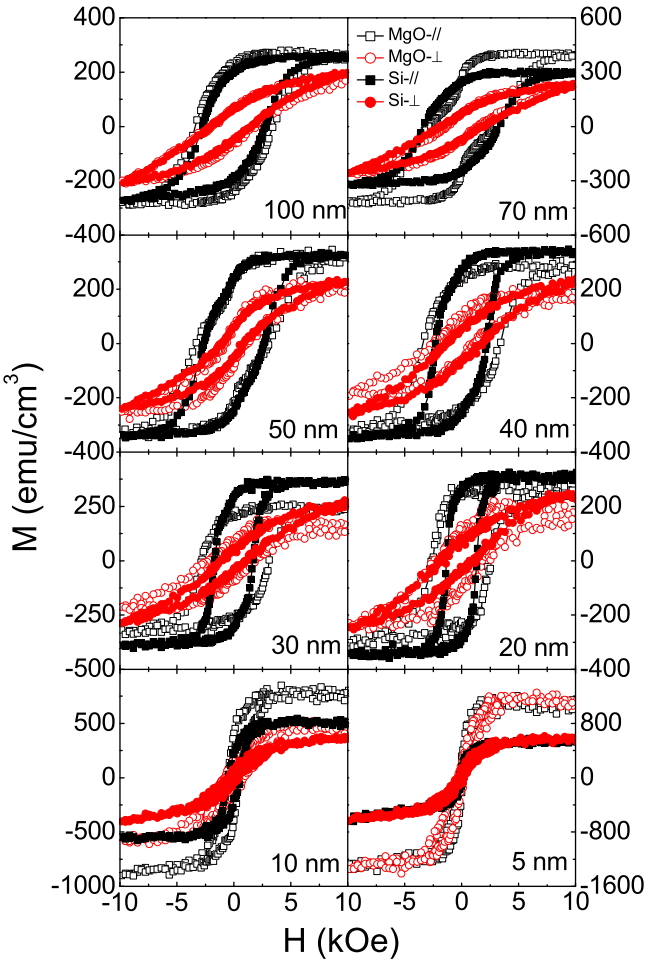


**Fig. 6.** $M$–$H$ curves of the $Fe_{56}Pt_{44}$-C granular films annealed at 550 °C with different $t$.

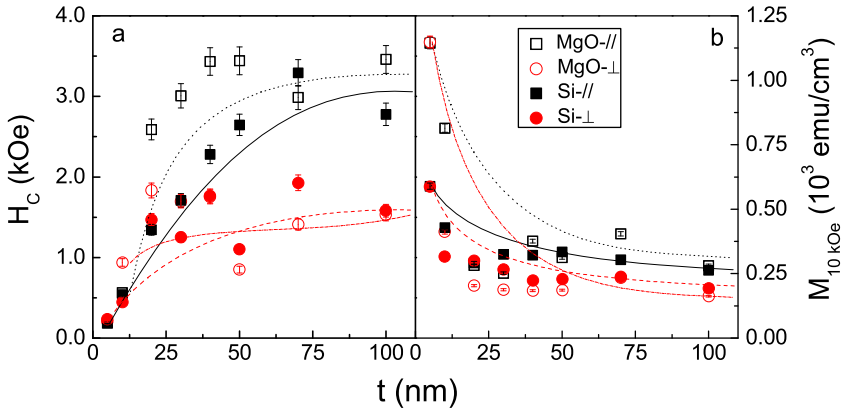


**Fig. 7.** Film-thickness dependence of the (a) coercivity and (b) saturation magnetization of the $Fe_{56}Pt_{44}$-C granular films annealed at 550 °C. The lines are the guides to the eyes.

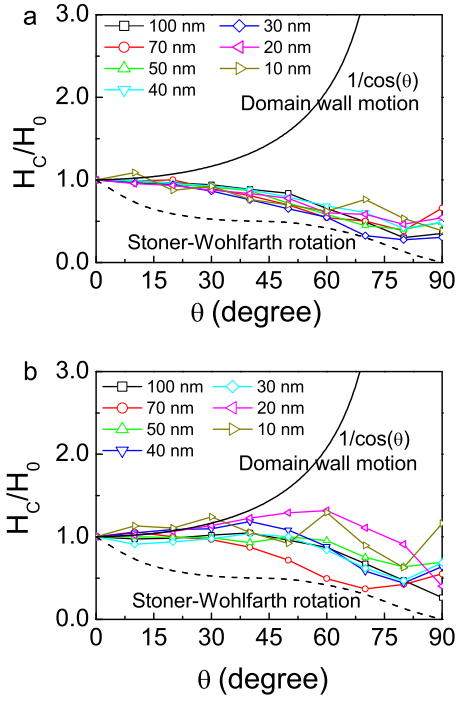


**Fig. 8.** Angular dependence of the coercivity of the $Fe_{56}Pt_{44}$-C granular films annealed at 550 °C with different $t$ on (a) MgO(1 0 0) and (b) $SiO_2$/Si(1 0 0) substrates.

the coercivity of the films will increase because the magnetocrystalline anisotropy should be almost the same for the ordered fct FePt grains.

Fig. 8 shows the angular dependence of the coercivity of the $Fe_{56}Pt_{44}$-C granular films with different $t$ on MgO(1 0 0) and $SiO_2$/Si(1 0 0) substrates annealed at 550 °C. From Fig. 8(a), the reversal mechanism of the films on MgO(0 0 1) substrates approaches the S–W rotation mode, suggesting that the ordered fct FePt grains are well separated by C matrix. However, the reversal mechanism of the films on the $SiO_2$/Si(1 0 0) substrates does not well approach the S–W rotation mode because of the interparticle interactions in the films. It also should be noted that the reversal mechanism of the films does not change with the increase of $t$.

## 4. Conclusions

The magnetic properties of the post-annealed $Fe_{1-x}Pt_x$-C granular films fabricated using a facing-target sputtering system with different $x$ and $t$ have been investigated systematically. The ordered fct FePt grains form as $x$ increases to a proper value. All of the films are ferromagnetic, and the easy axis of the films lies in the film plane. With the decreasing $t$, the films turn from hard ferromagnetic to soft ferromagnetic. The maximum coercivity of the 100-nm thick films at a 10-kOe field is 3.7 kOe at $x = 0.48$. The coercivity of the $Fe_{0.56}Pt_{0.44}$-C granular films increases, and the magnetization at a 10-kOe field decreases with the increase of the film thickness. The reversal mechanism of the films turns from the domain wall motion to the S–W rotation mode as $x$ increases. Meanwhile, the reversal mechanism of the $Fe_{56}Pt_{44}$-C granular films with the S–W rotation mode is not film-thickness dependent.

## Acknowledgements

This work was supported by NSFC of China (50701033), the RFDP (20070056047), TSTC (08JCYBJC09400) and Young Faculty Foundation of Tianjin University (TJU–YFF–08B52 and 08A05).

## References

[1] B. Zhang, W.A. Soffa, Scr. Metall. 30 (1994) 683.
[2] T.J. Klemmer, D. Hoydick, H. Okumura, B. Zhang, W.A. Soffa, Scr. Metall. 33 (1995) 1793.
[3] H. Kanazawa, G. Lauhoff, T. Suzuki, J. Appl. Phys. 87 (2000) 6143.
[4] S.H. Sun, C.B. Murray, D. Weller, L. Folks, A. Moser, Science 287 (2000) 1989.
[5] W.B. Mi, J.J. Shen, W.J. Lu, H.L. Bai, J. Alloys Compd. 503 (2010) 233.
[6] Y.K. Takahashi, K. Hono, J. Appl. Phys. 84 (2004) 383.
[7] J.M. Qiu, J.P. Wang, Appl. Phys. Lett. 88 (2006) 192505.
[8] R.A. Ristau, K. Barmak, L.H. Lewis, K.R. Coffy, J.K. Howard, J. Appl. Phys. 86 (1999) 4527.
[9] C.M. Kuo, P.C. Kuo, H.C. Wu, J. Appl. Phys. 85 (1999) 2264.
[10] W.B. Mi, H. Liu, Z.Q. Li, P. Wu, E.Y. Jiang, H.L. Bai, J. Appl. Phys. 97 (2005) 124303.
[11] S.S.K. Kamal, P.K. Sahoo, L. Durai, P. Ghosal, S. Ram, M. Raja, J. Alloys Compd. 501 (2010) 297.
[12] J.S. Chen, B.C. Lim, Y.F. Ding, J.F. Hu, G.M. Chow, G. Ju, J. Appl. Phys. 105 (07) (2009) B702.
[13] B. Ma, C.L. Zha, Z.Z. Zhang, Q.Y. Jin, Thin Solid Films 518 (2010) 2163.
[14] R.J. Tang, W.L. Zhang, Y.R. Li, J. Alloys Compd. 496 (2010) 380.
[15] B.C. Lim, J.S. Chen, J.F. Hu, P.W. Lwin, Y.F. Ding, K.M. Cher, B. Liu, J. Appl. Phys. 105 (07) (2009) A730.
[16] Y.H. Fang, P.C. Kuo, A.C. Sun, S.L. Hsu, S.C. Chen, Thin Solid Films 517 (2009) 5181.
[17] W.Y. Zhang, H. Shima, F. Takano, H. Akinaga, X.Z. Yu, T. Hara, W.Z. Zhang, K. Kimoto, Y. Matsui, S. Nimori, J. Appl. Phys. 106 (2009) 033907.
[18] T. Hasegawa, J. Miyahara, T. Narisawa, S. Ishio, H. Yamane, Y. Kondo, J. Ariake, S. Mitani, Y. Sakuraba, K. Takanashi, J. Appl. Phys. 106 (2009) 103928.
[19] J.L. Tsai, G.B. Lin, H.T. Tzeng, J. Alloys Compd. 487 (2009) 18.
[20] K.F. Dong, X.F. Yang, J.B. Yan, W.M. Cheng, X.M. Cheng, X.S. Miao, X.H. Xu, F. Wang, J. Alloys Compd. 476 (2009) 662.
[21] Y. Inaba, G.B. Thompson, J.W. Harrell, T. Klemmer, Y. Kubota, J. Appl. Phys. 107 (2010) 053507.
[22] J.Q. Zhao, B.Y. Cui, Z.Z. Zhang, B. Ma, Q.Y. Jin, Thin Solid Films 518 (2010) 2830.
[23] B. Laenens, F.M. Almeida, N. Planckaert, K. Temst, J. Meersschaut, A. Vantomme, C. Rentenberger, M. Rennhofer, B. Sepiol, J. Appl. Phys. 105 (2009) 073913.
[24] X.H. Li, F.Q. Wang, Z. Guo, H. Li, D.F. Guo, B.T. Liu, X.Y. Zhang, Appl. Surf. Sci. 256 (2010) 3822.

[25] R.S. Ruoff, D. Lorents, B. Chan, R. Malhotra, S. Subramoney, Science 259 (1993) 346.
[26] W.B. Mi, H. Liu, Z.Q. Li, P. Wu, E.Y. Jiang, H.L. Bai, Appl. Surf. Sci. 252 (2006) 8688.
[27] J. Sangki, Y.N. Hsu, D.E. Laughlin, M.E. McHenry, IEEE Trans. Magn. 36 (2000) 2336.
[28] S. Chikazumi, Physics of Ferromagnetism, Clarendon, Oxford, 1997.
[29] L. Zhang, A. Manthiram, Phys. Rev. B 54 (1996) 3462.
[30] J. Arcas, A. Hernando, J.M. Barandiaran, C. Prados, M. Vazquez, P. Marın, A. Neuweiler, Phys. Rev. B 58 (1998) 5193.
[31] E.C. Stoner, E.P. Wohlfarth, IEEE Trans. Magn. 27 (1991) 3475.